Interference in climbing a quantum ladder system with frequency-chirped laser pulses

P. Balling,[1,2] D. J. Maas,[1] and L. D. Noordam[1]
[1]*FOM–Institute for Atomic and Molecular Physics, Kruislaan 407, 1098 SJ Amsterdam, The Netherlands*
[2]*Institute of Physics and Astronomy, University of Aarhus, 8000 Aarhus C, Denmark*
(Received 11 March 1994)

Excitation of a quantum ladder system by frequency-swept (-chirped) laser pulses has been investigated by studying an atomic model system, the $5s$-$5p$-$5d$ ladder of rubidium. The population transfer is significantly enhanced when the frequency is swept such that it follows the spacing of the ladder. At intermediate intensities we observe oscillations in the population transfer to the upper level ($5d$), which can be attributed to interference between two routes of excitation: sequential transfer and direct two-photon excitation via a virtual intermediate state. We determine simultaneously the population transfer to the upper level ($5d$) and the direct three-photon ionization, the latter corresponding to a three-step ladder with the final state being in the continuum: $5s$-$5p$-$5d$-$\varepsilon p/\varepsilon f$. Experiments were performed, using 100 fs pulses at $\sim$780 nm from a self-mode-locked Ti:Al_2O_3 oscillator amplified at 10 Hz.

PACS number(s): 42.50.Hz, 32.80.Bx, 42.65.Re

I. INTRODUCTION

The quest of manipulating quantum systems on a detailed level, thus controlling the exact quantum state of the system, has been long ongoing. The advent of the laser facilitated high selectivity in the interaction with atomic and molecular systems, but it is only through recent theoretical and experimental developments that the goal is becoming realistic for more complicated systems [1]. One important example of quantum manipulation is the attempt to bring an ensemble of molecules into a specific highly excited vibrational state. This facilitates the selective breaking of chemical bonds, thus modifying chemical reactions [2,3]. Direct single-photon excitation to a highly excited vibrational state is not possible, due to the small overlap between the initial and final states. Thus a stepwise excitation is needed, introducing other complications. The anharmonicity of the chemical bond results in different transition frequencies between sequential vibrational states, demanding the use of several laser frequencies. Furthermore, the time scales for redistribution of vibrational energy within a molecule are very short (picosecond range). Ultrashort laser pulses can potentially present a solution to both of these problems, since the bandwidth of ultrashort pulses may be large enough to contain all the frequency components needed in the vibrational ladder, and picosecond time resolution is readily obtained. At a first glance it may seem that selectivity cannot be sustained with this approach, and even if the purpose is simply multiphoton dissociation it turns out that the intensities needed to dissociate an appreciable fraction of the molecules are far beyond those leading to ionization.

A possible solution to the problem was suggested by Chelkowski, Bandrauk, and Corkum [4]. They proposed to use chirped (or frequency-swept) ultrashort laser pulses. If the laser pulse is blue to red chirped, the instantaneous frequency will follow the spacing between the vibrational levels of the anharmonic molecular potential. The process suggested is an example of chirped adiabatic passage. Adiabatic passage is an attractive approach for obtaining efficient population transfer [1,5], primarily because of the insensitivity to inhomogeneities associated with the ensemble of molecules, as compared, for example, to Rabi pumping. Adiabatic passage by chirped pulses has been used to create inversion in a collection of molecules, with more than half of the population being transferred to an excited electronic and rovibronic state [6]. A high degree of selectivity has been proven to be compatible with the large bandwidth of a short laser pulse [7]. Adiabatic passage in a molecular vibrational ladder system has yet to be demonstrated. In a recent paper population transfer by chirped pulse adiabatic passage has been investigated in an atomic model system, the three-state ladder $5s \rightarrow 5p \rightarrow 5d$ in the rubidium atom [8].

In this paper we will show that in the three-level ladder system of rubidium, the actual population transfer at moderate intensities is oscillating as a function of the chirp due to quantum interference. A simplified energy-level diagram of Rb is depicted in Fig. 1(a). We label the $5s$, $5p$, and $5d$ states $|1\rangle$, $|2\rangle$, and $|3\rangle$, respectively. In the experiment Rb atoms interact with laser pulses of a bandwidth large enough to contain the photon energies corresponding to both transitions of the ladder system, $5s \rightarrow 5p$ (12 817 cm^{-1}) and $5p \rightarrow 5d$ (12 885 cm^{-1}). The dependence of the population transfer to the upper level $|3\rangle$ on the frequency chirp of the laser is investigated. It is found that the population transfer is enhanced when the applied pulse is red to blue chirped (positively chirped). This is to be expected, since the $|1\rangle \rightarrow |2\rangle$ transition is resonant in the beginning of the pulse, and the $|2\rangle \rightarrow |3\rangle$ transition becomes resonant at a later time during the pulse.

The effect of chirping the optical pulses on the population transfer can be visualized using the dressed-atom picture. In Fig. 1(b) the dashed lines show the unperturbed dressed atom states of $|1+\hbar\omega\rangle$, $|2\rangle$, and

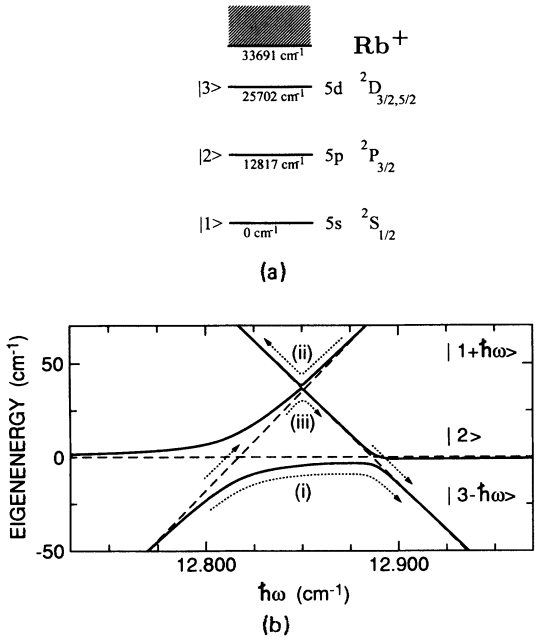

FIG. 1. (a) A simplified energy-level diagram of rubidium. The $5s \leftrightarrow 5p$ (or $|1\rangle \leftrightarrow |2\rangle$) and $5p \leftrightarrow 5d$ ($|2\rangle \leftrightarrow |3\rangle$) couplings can be driven by the same ultrashort laser pulse, due to the small difference in the energy spacings. (b) Dressed-atom diagram of the same levels, dressed as $|1+\hbar\omega\rangle$, $|2\rangle$, and $|3-\hbar\omega\rangle$. The dashed lines show the unperturbed energies vs the photon energy of the dressing field. The full lines show the dressed-atom energies, when the dipole coupling is included, and the laser has an intensity of 1.9×10^7 W/cm^2. The arrows indicate different routes of excitation of the upper level ($5d$), as described in the text.

$|3-\hbar\omega\rangle$, and their energy dependence on the photon energy. Including the dipole coupling between states $|1\rangle \leftrightarrow |2\rangle$ and $|2\rangle \leftrightarrow |3\rangle$ the dressed-atom states split up [full lines in Fig. 1(b)]. In a chirped pulse the instantaneous frequency changes during the pulse, which correspond to a traversal of the dressed-atom diagram from left to right (red to blue chirped) or right to left (blue to red chirped). Depending on the strength of the dipole coupling (determined by intensity) and the rate of the frequency sweep (determined by the chirp), the avoided crossings of the dressed states are traversed more or less adiabatically. If the frequency chirp is from red to blue [left to right in Fig. 1(b)], population transfer from level 1 to level 3 occurs if an atom follows the full (adiabatic) dressed-atom curve [route marked (*i*)]. This is the so-called intuitive frequency chirp leading to efficient population of the upper state. Note that once the intensity is high enough to traverse the crossings fully adiabatically, the population transfer will still be 100% for all higher intensities. This is in contrast to Rabi pumping, where the upper-state population keeps oscillating as a function of intensity. In a recent paper the 100% population transfer was demonstrated experimentally [8]. That paper also showed that at sufficiently high intensities, even with a counter intuitive chirp (blue to red), 100% of the population can be transferred [route (*ii*) in Fig. 1(b)]. The previous experiment was performed using very intense pulses with a square power spectrum. In the present experiment only Gaussian pulses with a lower intensity are involved. As to be expected, no complete population transfer is found at the moderate intensities we used.

However, at these intermediate intensities a third, new, route leading to population of level 3 becomes of importance. If an atom is dressed by a red to blue chirped light field, it may follow $|1+\hbar\omega\rangle$ crossing $|2\rangle$ diabatically, then going adiabatically to $|3-\hbar\omega\rangle$ and continuing in this state crossing level $|2\rangle$ a second time [route (*iii*) on Fig. 1(b)]. The relative significance of routes (*i*) and (*iii*) depends on the experimental parameters (Sec. IV). In general, a (quantum-mechanical) interference between the two pathways is expected. This interference manifests itself as oscillations in the population transfer versus chirp, and is a general feature in most of our measurements as well as in the calculated results (see Sec. VI). The accumulated phase difference between the two paths depends on the difference in energy and the time spent to traverse the paths. For a linearly chirped pulse this time is proportional to the chirp, and the phase change is simply the product of the area between the two paths [Fig. 1(b)] and the chirp, giving regular oscillations as a function of the chirp (Sec. III).

After the population transfer to level 3 another photon can be absorbed to leave the atom ionized. This process corresponds to a four-level ladder, with the last level being in the continuum. The situation is analogous to a molecular ladder ending up in a dissociative state. The three-photon ionization signal is primarily an image of the population in the upper bound state ($5d$), except at small chirp (high intensity), where a significant part of the signal seems to originate from direct off-resonant multiphoton ionization.

The paper is organized as follows: In Sec. II we will describe the experimental setup, and our key experimental findings are discussed qualitatively in Sec. III. Before the quantitative treatment of the results in Sec. VI, we discuss the experimental realization of chirped pulses in Sec. IV and a theory based on solving the Schrödinger equation in Sec. V.

II. DESCRIPTION OF THE EXPERIMENT

Rubidium atoms are evaporated into the interaction region of a vacuum system [9]. Across the interaction region a small voltage can be applied to accelerate detached electrons toward a channel electron multiplier. In the interaction region the atomic beam is crossed perpendicularly with the linearly polarized, collimated laser beam (Fig. 2). The laser source is based on a homebuilt Ti:Al_2O_3 oscillator. The self-mode-locked oscillator is running at $\sim$780 nm with a bandwidth of 10 nm and a pulse duration of 100 fs, i.e., approximately transform-limited pulses. Following spatial filtering the infrared (IR) laser pulses are amplified at 10 Hz in three Bethune cells containing LDS 765 (2-mm-diameter cell), LDS 798 (3-mm-diameter cell), and LDS 765 (8-mm-diameter cell), respectively. When pumped by the second harmonic of a

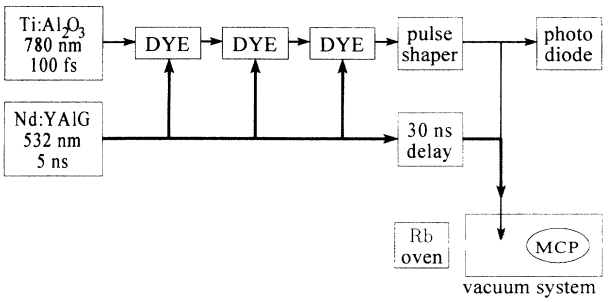

FIG. 2. A schematic of the experimental setup showing the laser system, pulse shaper, and the multi channel plate (MCP) detector in the vacuum chamber.

Q-switched Nd:YAlG (yttrium aluminum garnet) laser (pulse duration 8 ns), the overall average gain in the three cells is $\sim 10^5$, leading to amplified pulses of $\sim 50\ \mu J$. The amplified pulses are sent through a pulse shaper [10], which is used to change continuously the chirp of the IR pulses. A pulse shaper consists basically of two parallel gratings of a variable separation [Fig. 3(a)]. In order to be able to apply chirp in *both* directions, it is, however, necessary to add a $-1\times$ telescope between the two gratings [Fig. 3(b)]. The shaper was in fact implemented by using just one grating, an achromatic positive lens and a mirror in the configuration shown in Fig. 3(c). The distance between the lens and the mirror is fixed at the focal distance of the lens, while the grating can be displaced out of the focus plane. When the grating is moved away from the focus of the lens, the phase shift of a laser pulse is dependent on the frequency, i.e., chirp is induced. In the situation shown in Fig. 3, the distance between the grating and the lens is *larger* than the focus length, and the pulse shaper works like a normal grating compressor, having a phase shift decreasing with frequency, so that an initially unchirped pulse becomes blue to red (or negatively) chirped. A thorough description of the actual chirp as a function of the grating lens distance is given in Sec. IV.

The IR laser beam, which is kept collimated through the vacuum chamber, has a diameter of 3 mm. It is overlapped with a 2-mm-diameter green laser beam, being a fraction of the second harmonic of the Nd:YAlG laser, delayed approximately 30 ns. The probe laser postionizes Rb atoms which are left in the $5d$ state after interaction with the IR pulse. Since the probe laser has a smaller diameter than the IR beam, it only probes the central region of the IR laser, having approximately constant intensity. The relatively large delay of the postionizing laser serves to separate in time the electron signal stemming from direct three-photon ionization by the IR laser and from postionization. Since the lifetime of level 3 is 230 ns [11], the decay out of the $5d$ state before the arrival of the probe laser can be neglected. The fluence of the probe laser is generally chosen fairly low ($\sim 3\ J/m^2$) in order to keep the electron signal from the two different processes on the same order, to facilitate the simultaneous detection, and to avoid direct two-photon ionization of atoms in the ground ($5s$) or intermediate state ($5p$).

For each IR laser pulse the time-of-flight spectrum of the electron multiplier is recorded on a digital scope and transferred to a computer, and both the direct three-photon ionization and the post-ionization signals are collected. Due to the unseeded nature of the Nd:YAlG laser, the intensity and thus the gain in the Bethune cells at the instant of the short pulse fluctuates from shot to shot, leading to similar fluctuations in the pulse energy of the amplified pulses. The pulse energy of each shot of the IR laser is monitored on a photodiode, to serve for binning the two different ionization signals. For each value of the chirp (i.e., for each position of the shaper) typically 500 time-of-flight traces are recorded. The energy of the IR pulses after the shaper are typically a few tens of a microjoule, corresponding to fluences of $\sim 100\ \mu J/cm^2$.

Figure 4 shows an example of the signal measured by

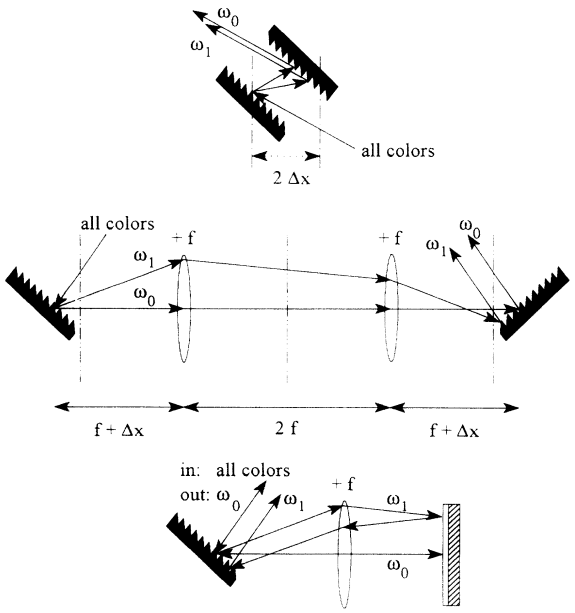

FIG. 3. This figure shows the working principle of the pulse shaper. In panel (a) a grating compressor is shown. The lines symbolize traces. Δx is the grating displacement. A $(-1\times)$ telescope is added in (b). Focal planes are indicated by $-\cdots-\cdots-$ lines. Now Δx can also be negative. In panel (c) the mirror images the second grating, thus reducing the setup.

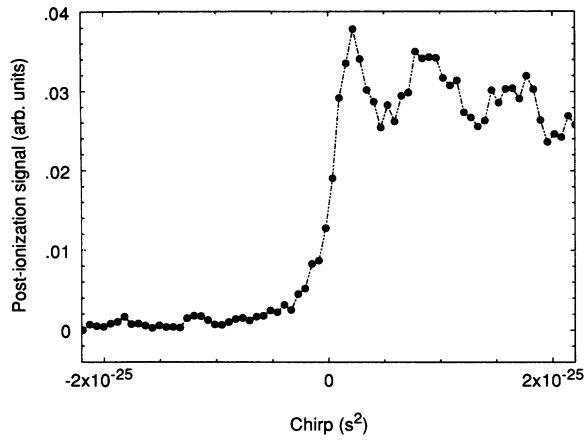

FIG. 4. The measured post-ionization signal vs the chirp of the IR laser pulse at a fluence of 120 μJ/cm^2 and a central wavelength of 780.0 nm ($\hbar\omega = 12\,821$ cm^{-1}). This signal is proportional to the population of the upper level ($5d$) after the pulse.

postionization of the Rb atoms upon interaction with an IR laser pulse of the indicated chirp. The chirp is calculated from the displacement of the grating, as described in Sec. IV. Strong enhancement in the population transfer is observed, when the IR pulse has a positive (red to blue) chirp. This agrees with the intuitive picture of the $|1\rangle \rightarrow |2\rangle$ transition being resonant before the $|2\rangle \rightarrow |3\rangle$ transition.

III. INTERFERENCE IN THE UPPER-STATE POPULATION

In order to understand the quantitative behavior of the interaction of the chirped pulses with the rubidium atoms, in Sec. V we will compare with a detailed theoretical model, based on integration of the time-dependent Schrödinger equation. The present section, however, is, devoted to the explanation of an interesting feature, common to all our measurements. Figure 4 shows that there is an oscillatory dependence of population transfer on the chirp for positive chirp. This is due to interference between the two paths leading to population of the d level [as shown in Fig. 1(b)]. The interference is a result of the intermediate intensity regime of this experiment: The avoided crossings are traversed neither fully diabatically nor fully adiabatically.

The intermediate intensity also results in less than the 100% population transfer reported earlier [8]. The criterion for a passage to be fully adiabatic is (for a two-level system [12]) that

$$\frac{d\theta}{dt} \ll \sqrt{\Omega(t)^2+\Delta(t)^2} , \tag{1}$$

where $\Omega(t)$ is the Rabi frequency, $\Delta(t)$ the time-dependent detuning, and $\theta(t)=\pi/2+\arctan(\Omega(t)/\Delta(t))$ is the polar angle of the Bloch vector. For a linear frequency chirp, the time-dependent detuning has the form $\Delta(t)=\Delta(0)+(d\omega/dt)t$, where $d\omega/dt$ is constant and $\Delta(0)$ is the difference between the central frequency of the light pulse, ω_0, and the transition frequency between the two levels under consideration. If the influence is high enough to saturate the transition ($\Omega\tau \sim 1$), the adiabatic criterion (1) can in principle always be met for a two-level system, if the carrier frequency is close to the transition and the chirp is large enough. In our ladder system, however, the two steps have a slight difference in transition frequencies, $\delta=(\omega_3-\omega_2)-(\omega_2-\omega_1)$, leading to fairly large detunings for either transition ($\hbar\delta \sim 63$ cm^{-1}). In this case the Rabi frequency has to be large, even for nonzero chirp, in order for the adiabatic criterion to be fulfilled, and that is not the case in this experiment.

The period of the interference wiggles can be explained by simple phase arguments. The two different paths correspond to different dressed-atom energies W, and since the wave function contains a factor $\exp(iWt)$, the phase of the upper-state wave function created by the two different routes is different. The period of the interference corresponds to phase changes of 2π. If we use $W_{(i)}$ and $W_{(iii)}$ for the dressed-atom energies of the two paths [corresponding to the notation of Fig. 1(b)], the accumulated phase difference is

$$\phi = \int_{t_1}^{t_2} [W_{(iii)}(t) - W_{(i)}(t)]dt , \tag{2}$$

where t_1 and t_2 are the times of the *diabatic* crossings going to path (*iii*). For a Gaussian pulse the instantaneous frequency changes linearly with time, so changing the variable of integration we obtain

$$\phi = \frac{1}{d\omega/dt} \int_{\omega(t_1)}^{\omega(t_2)} [W_{(iii)}(\omega) - W_{(i)}(\omega)]d\omega , \tag{3}$$

where $d\omega/dt$ is constant for a given pulse, but depends on the chirp, called α (see Sec. IV). Formula (3) shows that the phase difference is simply the ratio of the area between the two paths of Fig. 1(b) and the rate of change of the instantaneous frequency. The two instants of transition t_1 and t_2 are not really well defined, but at low intensity (e.g., at fairly large chirp), the dressed-atom energies are approximately equal to the unperturbed ones [dashed lines of Fig. 1(b)], and it is a good approximation to assume diabatic crossings at the time of the level crossings. In this case the area in formula (3) is that of a triangle of height $\delta/2$ and baseline δ, so that a phase change of 2π corresponds to

$$2\pi = \frac{1}{d\omega/dt} \frac{1}{2} \frac{\delta}{2} \delta , \tag{4}$$

or, using the fact that for large chirp $d\omega/dt \approx 1/(2\alpha)$ (see Sec. IV),

$$\alpha_{2\pi} = \frac{4\pi}{\delta^2} = 7.6\times 10^{-26}\ \text{s}^2 . \tag{5}$$

This estimate can now be compared with our experimental results. Quite generally the first oscillation (including the zero chirp region) has a period which is considerably smaller than the estimate of (5), cf. Fig. 4. This is expected, since the derivation was based on a large chirp. Using the same picture, however, the fact that the period drops leads us to the conclusion that the enclosed area in-

creases, which can be understood as the dressed-atom levels splitting up in the stronger field. This argument depends, of course, critically on the instants of the diabatic crossings. When we disregard the first oscillation, the remaining periods of oscillation agree exactly with the estimate of (5), except that there is a tendency that at high fluences the period decreases slightly, in agreement with the above argument.

A more naive look at the interference is that it originates from two different two-photon transition schemes. First, the atom can be excited sequentially by the chirped pulse at the instants where the frequency is resonant with the corresponding transition. Second, there is the possibility of direct two-photon excitation via a virtual state. This will take place when the photon energy is such that two photons match the energy difference between levels $|3\rangle$ and $|1\rangle$. As in the dressed-atom picture, the phase difference between the two transition schemes can be calculated, resulting in the same period as given in (5).

IV. CHIRP INTRODUCED BY THE PULSE SHAPER

The absolute value of the chirp, which is induced by the pulse shaper, can be calculated directly from experimental conditions. If we denote the displacement of the grating from the focal plane by Δx (Δx being positive if the distance is larger than the focal length, Fig. 3), then the distance between the two virtual gratings in the reduced system is $2\Delta x$. A light beam of wavelength λ approaching the grating under an incident angle i with respect to the normal will be diffracted to the angle r according to the well-known grating formula

$$\sin(i)+\sin(r)=m\frac{\lambda}{d} , \tag{6}$$

with d being the groove spacing of the grating and m the order of diffraction (in the present case m is 1 and -1 on the first and second gratings, respectively). The total phase shift experienced by the light beam traveling through the shaper is determined by both the (wavelength-dependent) path length l as well as by the phase shift which originates from the fact that there is a phase difference $2\pi m$ between consecutive grooves of the grating. The number of grooves to be included depends on wavelength, and is the ratio of the distance that the beam travels along the second grating to the groove spacing, i.e., $\cos(r_0)2\Delta x\tan(r)/d$, with r_0 being the fixed angle between the grating normal and the direction perpendicular to the mirror of the shaper. Accordingly, the total phase shift is

$$\phi(\lambda)=2\pi\frac{l}{\lambda}+2\pi m\cos(r_0)2\Delta x\tan(r)/d \tag{7}$$

or, using geometrical identities and the grating formula (6),

$$\phi(\omega)=\frac{2\cos(r_0)\omega}{c}[\cos(r)+\cos(i)]\Delta x . \tag{8}$$

An incident light pulse of spectrum $E_0(\omega)$ will leave the shaper as $E_0(\omega)\exp(i\phi(\omega))$. For a light pulse, which is centered around ω_0 having a reasonably small bandwidth [13], the total phase shift can be expanded around ω_0 to second order in ω:

$$\phi(\omega)\simeq\phi(\omega_0)+\frac{1}{1!}\frac{\partial\phi}{\partial\omega}\bigg|_{\omega=\omega_0}(\omega-\omega_0)+\frac{1}{2!}\frac{\partial^2\phi}{\partial\omega^2}\bigg|_{\omega=\omega_0}(\omega-\omega_0)^2 . \tag{9}$$

$\phi(\omega_0)$ is the phase shift of the carrier frequency within the pulse, while $\partial\phi/\partial\omega$ determines the group velocity of the pulse envelope. The first nontrivial term of equation (9) is the second-order term, which is responsible for group-velocity dispersion. In fact

$$\alpha=\frac{1}{2!}\frac{\partial^2\phi}{\partial\omega^2}\bigg|_{\omega=\omega_0} \tag{10}$$

is the quantity describing the amount of chirp introduced in the pulse shaper. If we take ϕ from Eq. (8), with r and i depending on ω through the grating formula (6), we obtain

$$\alpha=-\frac{4\pi^2c}{d^2}\frac{1}{\omega_0^3}\frac{1}{\cos^2(r_0)}\Delta x . \tag{11}$$

It appears that α is fixed by the experimental parameters, and for a given light pulse (fixed ω_0) the induced chirp is linear in the displacement of the grating.

In the experiment the incoming pulse is a Gaussian of pulse duration τ_0:

$$E_{\text{in}}(t)=\exp\left[-2\ln2\left[\frac{t}{\tau_0}\right]^2\right]\exp(i\omega_0t) , \tag{12}$$

which, when assumed to be bandwidth limited, has a bandwidth $\Delta\omega=4\ln2/\tau_0$, so that in the frequency domain

$$E_{\text{in}}(\omega)=\exp\left[-2\ln2\left[\frac{\omega-\omega_0}{\Delta\omega}\right]^2\right] . \tag{13}$$

If we include only the second-order phase change, the outgoing pulse becomes

$$E_{\text{out}}(\omega)=E_{\text{in}}\exp[i\alpha(\omega-\omega_0)^2]=E_{\text{in}}\exp\left[-\frac{(\omega-\omega_0)^2}{4\Gamma}\right] , \tag{14}$$

where Γ is given by

$$\Gamma=\left[\frac{8\ln2}{\Delta\omega^2}+4i\alpha\right]^{-1} . \tag{15}$$

The time dependence of the outgoing pulse is

$$E_{\text{out}}(t)=\exp(-\Gamma t^2)\exp(i\omega_0t) . \tag{16}$$

This pulse is also Gaussian, but with a pulse duration which depends on the chirp:

$$\tau^2=\tau_0^2+\left[\frac{8\ln 2\alpha}{\tau_0}\right]^2, \tag{17}$$

i.e., for $\alpha \gg \tau_0^2$ the pulse is stretched approximately linearly with the chirp. The instantaneous frequency changes linearly in time during the pulse, with the rate of change $d\omega/dt$ being approximately inversely proportional to the chirp α:

$$\omega(t)=\omega_0+\frac{\alpha\left[\frac{\Delta\omega^2}{\ln 2}\right]^2}{8+2\alpha^2\left[\frac{\Delta\omega^2}{\ln 2}\right]^2}t\ . \tag{18}$$

To summarize, the shaper introduces a chirp which is quadratic in the frequency domain and hence *for Gaussian pulses* linear in the time domain [14].

V. THEORETICAL MODEL

The rubidium three-level ladder system is modeled by solving the time-dependent Schrödinger equation in a truncated basis. We include only states that are within the bandwidth of our laser, i.e., the $5s\ ^2S$, the $5p\ ^2P_{3/2}$, and the two fine-structure components of the $5d$ state, $^2D_{3/2}$ and $^2D_{5/2}$. While keeping the notation $|1\rangle$ and $|2\rangle$ for the included $5s$ and $5p$ states, for convenience we label the $^2D_{3/2}$ and $^2D_{5/2}$ by $|3\rangle$ and $|4\rangle$, and denote continuum states as $|\varepsilon\rangle$. Figure 5(a) shows the states and couplings included in the model.

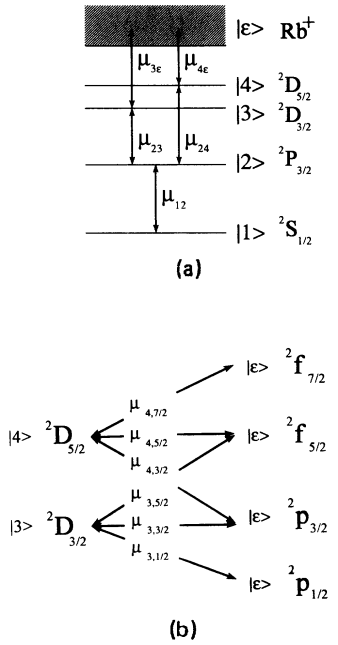

FIG. 5. (a) Energy-level diagram of rubidium, showing the levels and the couplings included in the model described in the text. (b) A detailed picture of the coupling of the two $5d$ states to the continuum.

The unperturbed atomic system is described by

$$\begin{aligned} H_0|n\rangle&=\hbar\omega_n|n\rangle\ ,\\ H_0|\varepsilon\rangle&=\hbar\omega_\varepsilon|\varepsilon\rangle\ , \end{aligned} \tag{19}$$

while the full Hamiltonian in the dipole approximation has the form ($\mathbf{D}=-e\mathbf{r}$)

$$H=H_0-\mathbf{D}\cdot\mathbf{E} \tag{20}$$

to be used in the Schrödinger equation.

The wave function can be expanded in the above basis as

$$i\hbar\frac{\partial\Psi}{\partial t}=H\Psi\ , \tag{21}$$

$$\Psi=\sum_n \exp(-i\omega_n t)a_n(t)|n\rangle + \sum_\varepsilon \exp(-i\omega_\varepsilon t)a_\varepsilon(t)|\varepsilon\rangle\ . \tag{22}$$

In our calculations below, the sum (integral) over continuum states $|\varepsilon\rangle$ will be eliminated. By substituting expression (22) for Ψ into the Schrödinger equation (21) and multiplying with $\langle n|$ and $\langle\varepsilon|$, respectively, we obtain

$$\begin{aligned} i\hbar\exp(-i\omega_n t)\dot{a}_n(t) &= \sum_{n'}\exp(-i\omega_{n't})a_{n'}(t)\langle n|\mathbf{E}\cdot\mathbf{D}|n'\rangle \\ &\quad+\sum_{\varepsilon'}\exp(-i\omega_{\varepsilon' t})a_{\varepsilon'}(t)\langle n|\mathbf{E}\cdot\mathbf{D}|\varepsilon'\rangle\ , \\ i\hbar\exp(-i\omega_\varepsilon t)\dot{a}_\varepsilon(t) &= \sum_{n'}\exp(-i\omega_{n't})a_{n'}(t)\langle\varepsilon|\mathbf{E}\cdot\mathbf{D}|n'\rangle \\ &\quad+\sum_{\varepsilon'}\exp(-i\omega_{\varepsilon' t})a_{\varepsilon'}(t)\langle\varepsilon|\mathbf{E}\cdot\mathbf{D}|\varepsilon'\rangle\ . \end{aligned} \tag{23}$$

In our model only levels $|3\rangle$ and $|4\rangle$ couple to the continuum, and furthermore it is reasonable to assume that continuum levels do not couple, since continuum-continuum processes (ATI) only become relevant at much higher intensities (e.g., 10^{12} W/cm^2) [15]. For the electric field of the laser pulse we take a Gaussian pulse, linearly polarized in the z direction:

$$\mathbf{E}(t)=E_0\mathbf{e}_z\tfrac{1}{2}[\exp(-\Gamma t^2)\exp(i\omega_0 t) + \exp(-\Gamma^* t^2)\exp(-i\omega_0 t)]\ . \tag{24}$$

Since $\omega_0\approx\omega_2-\omega_1\approx\omega_3-\omega_2\approx\omega_4-\omega_2$, we may use the rotating-wave approximation, and obtain

$$\dot{a}_1=\frac{eE_0}{2i\hbar}\exp(-\Gamma t^2)\exp[i(\omega_1-\omega_2+\omega_0)t]a_2\langle 1|z|2\rangle ,$$

$$\dot{a}_2=\frac{eE_0}{2i\hbar}\{\exp(-\Gamma^* t^2)\exp[i(\omega_2-\omega_1-\omega_0)t]a_1\langle 2|z|1\rangle$$
$$+\exp(-\Gamma t^2)\exp[i(\omega_2-\omega_3+\omega_0)t]a_3\langle 2|z|3\rangle+\exp(-\Gamma t^2)\exp[i(\omega_2-\omega_4+\omega_0)t]a_4\langle 2|z|4\rangle\} , \quad (25)$$

$$\dot{a}_3=\frac{eE_0}{2i\hbar}\left[\exp(-\Gamma^* t^2)\exp[i(\omega_3-\omega_2-\omega_0)t]a_2\langle 3|z|2\rangle+\exp(-\Gamma t^2)\sum_{\varepsilon'}\exp[i(\omega_3-\omega_{\varepsilon'}+\omega_0)t]a_{\varepsilon'}\langle 3|z|\varepsilon'\rangle\right] ,$$

$$\dot{a}_4=\frac{eE_0}{2i\hbar}\left[\exp(-\Gamma^* t^2)\exp[i(\omega_4-\omega_2-\omega_0)t]a_2\langle 4|z|2\rangle+\exp(-\Gamma t^2)\sum_{\varepsilon'}\exp[i(\omega_4-\omega_{\varepsilon'}+\omega_0)t]a_{\varepsilon'}\langle 4|z|\varepsilon'\rangle\right] .$$

For the continuum states, we have

$$\dot{a}_\varepsilon=\frac{eE_0}{2i\hbar}\{\exp(-\Gamma^* t^2)\exp[i(\omega_\varepsilon-\omega_3-\omega_0)t]a_3\langle\varepsilon|z|3\rangle+\exp(-\Gamma^* t^2)\exp[i(\omega_\varepsilon-\omega_4-\omega_0)t]a_4\langle\varepsilon|z|4\rangle\} . \quad (26)$$

This equation can be formally integrated and substituted into the equations for $\dot{a}_3$ and $\dot{a}_4$. If we assume that the continuum is flat (i.e., $\langle\varepsilon|z|n\rangle$is independent of ε) and infinitely wide, then the continuum can be adiabatically eliminated simply to give ionization out of the states $|3\rangle$ and $|4\rangle$ in addition to a coupling of the two states through the continuum. The situation is actually slightly more complicated, since there are in fact four different continua; $^2f_{7/2}$, $^2f_{5/2}$, $^2p_{3/2}$, and $^2p_{1/2}$, with only two of these, $^2f_{5/2}$ and $^2p_{3/2}$, being accessible from both $|3\rangle$ and $|4\rangle$ [Fig. 5(b)]. As it can be seen, the four continua can be uniquely labeled by their j quantum number, so we introduce the notation

$$\mu_{n,n'}=e\langle n|z|n'\rangle ,$$
$$\mu_{n,j}=e\langle n|z|\varepsilon j\rangle , \quad (27)$$

which leaves us with the equations

$$\dot{a}_3=\frac{E_0}{2i\hbar}\exp(-\Gamma^* t^2)\exp[i(\omega_3-\omega_2-\omega_0)t]\mu_{3,2}a_2$$
$$+\frac{K}{2}I(t)[(|\mu_{3,1/2}|^2+|\mu_{3,3/2}|^2+|\mu_{3,5/2}|^2)a_3+(\mu_{3,3/2}\mu^*_{4,3/2}+\mu_{3,5/2}\mu^*_{4,5/2})a_4]$$
$$\dot{a}_4=\frac{E_0}{2i\hbar}\exp(-\Gamma^* t^2)\exp[i(\omega_4-\omega_2-\omega_0)t]\mu_{4,2}a_2 \quad (28)$$
$$+\frac{K}{2}I(t)[(|\mu_{4,3/2}|^2+|\mu_{4,5/2}|^2+|\mu_{4,7/2}|^2)a_4+(\mu^*_{3,3/2}\mu_{4,3/2}+\mu^*_{3,5/2}\mu_{4,5/2})a_3] ,$$

where $I(t)=\frac{1}{2}c\varepsilon_0E_0^2|\exp(-\Gamma t^2)|^2$ is simply the time-dependent intensity of the Gaussian laser pulse, and the constant K, given in the Appendix, converts the square of the dipole matrix elements to partial cross sections in units of inverse fluence. If we assume pure LS coupling, the relative strengths of the different coupling matrix elements to the continuum can be determined using vector algebra [16] (see the Appendix). We then obtain the four coupled differential equations

$$\dot{a}_1=\frac{E_0}{2i\hbar}\exp(-\Gamma t^2)\exp[i(\omega_1-\omega_2+\omega_0)t]\mu_{1,2}a_2 ,$$

$$\dot{a}_2=\frac{E_0}{2i\hbar}\{\exp(-\Gamma^* t^2)\exp[i(\omega_2-\omega_1-\omega_0)t]\mu_{2,1}a_1$$
$$+\exp(-\Gamma t^2)\exp[i(\omega_2-\omega_3+\omega_0)t]\mu_{2,3}a_3+\exp(-\Gamma t^2)\exp[i(\omega_2-\omega_4+\omega_0)t]\mu_{2,4}a_4\} , \quad (29)$$

$$\dot{a}_3=\frac{E_0}{2i\hbar}\exp(-\Gamma^* t^2)\exp[i(\omega_3-\omega_2-\omega_0)t]\mu_{3,2}a_2+\tfrac{1}{2}I(t)\left[(\tfrac{51}{120}\sigma_p+\tfrac{7}{15}\sigma_f)a_3+\left[\frac{3}{20\sqrt{6}}\sigma_p+\frac{1}{15\sqrt{6}}\sigma_f\right]a_4\right] ,$$

$$\dot{a}_4=\frac{E_0}{2i\hbar}\exp(-\Gamma^* t^2)\exp[i(\omega_4-\omega_2-\omega_0)t]\mu_{4,2}a_2+\tfrac{1}{2}I(t)\left[(\tfrac{9}{20}\sigma_p+\tfrac{301}{630}\sigma_f)a_4+\left[\frac{3}{20\sqrt{6}}\sigma_p+\frac{1}{15\sqrt{6}}\sigma_f\right]a_3\right] ,$$

where σ_p and σ_f are the total (multiplet averaged) cross sections for ionization of the $5d$ state to the p and f continua, respectively.

The dipole moments $\mu_{n,n'}$ between bound states needed in the calculation can be derived from reported oscillator strengths [11] under the assumption of LS coupling. The values are given in Table I. In order to calculate the values of the ionization cross sections, we perform an estimate based on a Yukawa potential [17]. The two potential parameters are adjusted to reproduce reasonably the quantum defects of the p, d, and f series, as well as the position of a few lower-lying states. Based on the wave functions of this potential, we obtain approximate values for ionization to the p and f continua (Table I). Under the conditions of this experiment the fluence of the IR pulses are in all cases so low that saturation can be ignored. Therefore only the ratio σ_p/σ_f is important. The model potential estimate gives a ratio of $\sim 1/20$, which is in agreement with more advanced calculations performed on sodium at similar photon energies [18].

The set of equations (29) is solved numerically by integration over the duration of the frequency-chirped laser pulse, using Eq. (16). For a given chirp the population distribution over the four levels at the end of the IR laser pulse is determined. The three-photon ionization signal by the pulse is given by the population of continuum states, which can be calculated as the loss in the total population of the bound states. In order to facilitate comparison with the signal from the post-ionizing laser, the populations in levels $|3\rangle$ and $|4\rangle$ are weighted by the cross section for ionizing the respective level with the probe laser. In fact, since the cross sections predicted by our model calculation at the wavelength of the probe laser are the same within a few percent, we can compare the post-ionization signal with the sum of the population in the two upper levels.

VI. RESULTS AND DISCUSSION

Figure 6 shows a comparison of experimental and theoretical results for the post-ionization signal (proportional to the upper state population) at two different fluences. The experimental chirp is determined from the displacement of the pulse shaper, according to formula (11). The solid curve shows the signal which is expected, based on integration of the time-dependent Schrödinger equation, as described in Sec. V. Only the vertical scale of the experiment has been adjusted. The calculations show the same features as have already been discussed for the experimental results: The strong enhancement in the

TABLE I. List of atomic parameters. Dipole moments are derived from oscillator strengths quoted in [11]. Cross sections are determined by model potential calculations as described in the text.

$\mu_{1,2}$	2.03×10^{-29} C m
$\mu_{2,3}$	6.45×10^{-31} C m
$\mu_{2,4}$	4.74×10^{-30} C m
σ_p	3.8×10^{-4} m^2/J
σ_f	8.3×10^{-3} m^2/J

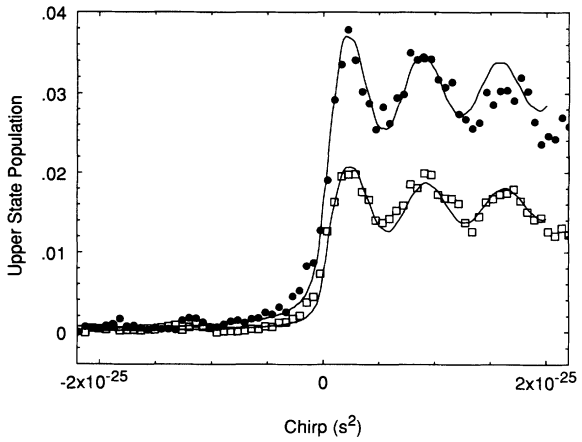

FIG. 6. A comparison of the population transfer to the upper level ($|3\rangle$ and $|4\rangle$), as measured by post-ionization (points) and predicted by the theoretical model (solid curves). Results are shown at two different fluences: 75 (lower curve) and 120 μJ/cm^2 (upper curve, similar to Fig. 3).

population transfer at positive chirp and the interference wiggles. Furthermore, the calculated results show that the population transfer to the upper d level, level $|4\rangle$ is more than an order of magnitude larger than the transfer to the level $|3\rangle$. This is due to the much stronger dipole coupling to this level, cf. Table I. It is a good approximation at the intermediate fluences of this experiment to disregard level $|3\rangle$, and this has been done in producing the simplified dressed-atom energy-level diagram of Fig. 1(b).

It can be seen from Fig. 6 that the relative amplitude of the interference wiggles to the total population transfer depends on the pulse fluence: The higher the fluence the smaller the relative amplitude of the wiggles. This can be explained as an increase in the adiabaticity of the traversal of the dressed-atom diagram at higher fluences. Hence a larger fraction of atoms will go through the fully adiabatic path [marked (i) on Fig. 1(b)]. So if this path is already dominant (which appears to be the case), the relative amplitude of the wiggles will decrease with increasing fluence. This in fact lends us an internal check of the experimental fluences. If the fluence is calibrated to give agreement between measured and calculated ratios of wiggle amplitude to peak height, we end up with a fluence, which deviates less than 15% from the experimentally estimated value.

A comparison of the measured three-photon ionization signal and the calculated population loss is shown in Fig. 7, again for two different fluences. Both experiment and calculation show oscillations versus chirp, reflecting the interference in the upper-state population. This indicates that (for the large chirp) the three-photon ionization by the IR laser pulse is dominated by the stepwise process of transfer to the d level, followed by ionization by the remaining fluence of the pulse. At higher fluences the region of small chirp is apparently not well described by our model. The discrepancy can probably be explained by the limited number of states included in the model,

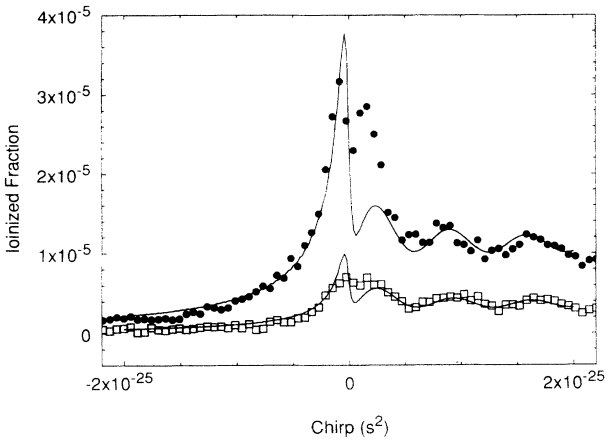

FIG. 7. A comparison of the three-photon ionization signal by the IR pulse under the same conditions as in Fig. 5.

since at high intensities off-resonant contributions from, for instance, the $5p\ ^2P_{1/2}$ (in the $|1\rangle \rightarrow |3\rangle$ transition) or the $7s\ ^2S_{1/2}$ (in the $|2\rangle \rightarrow |\varepsilon\rangle$ transition) may become important. As it appears from the vertical scales of Figs. 6 and 7, only a small fraction of the atoms being transferred to the upper state is actually ionized. This is of course due to the small overlap between a bound atomic state and the continuum. For a molecular ladder, however, it is much more probable to transfer a molecule from a highly excited vibrational state to the dissociation continuum.

The possibility of interfering routes is a quite general property of a quantum ladder system. In the dressed-atom picture it is easy to see that the number of enclosed areas increases rapidly with the number of levels N: There are potentially 2^{N-2} interfering routes. The importance of the interfering routes depends, however, critically on the strength of the interaction between the crossing levels. If the levels are only dipole coupled to nearby neighbors (as is approximately the case for the molecular ladder where the levels differ in vibrational quantum number) then the indirect coupling through intermediate levels drops rapidly when increasingly remote levels cross. This reduces the possible number of interfering routes. If we consider a quantum ladder having a monotonic change in the level spacing (e.g., the vibrational ladder of a molecule) and assume that a level only interacts significantly with its nearest and next-nearest neighbors, then the number of interferences is only $N-2$. In the alternative picture of sequential versus direct nonresonant population transfer (Sec. III), the different interfering pathways correspond to different steps of the ladder being direct (nonresonant) or sequential. The assumption of only nearest- and next-nearest-neighbor interaction corresponds to looking only at nonresonant *two-photon* transitions, neglecting higher-order processes that are not sequential.

It is important to notice that the interference phenomenon is not limited to excitation with Gaussian pulses. If the ladder system interacts with a chirped pulse of arbitrary envelope, interference wiggles will still be present. It is, however, only for a Gaussian pulse that a quadratic phase change corresponds to a linear chirp and hence induces oscillations of a constant period. Presumably the irregular oscillations observed in a previous experiment using square pulses were signatures of the same interference [8]. In the case of Gaussian pulses the interpretation is, however, much simpler, and it is possible to attribute oscillations of a certain period to an enclosed area in the dressed-atom diagram, thus yielding structural information about the ladder system.

VII. CONCLUSION

We have investigated population transfer in a three-level model system, identifying a general interference mechanism, which gives oscillations in the population transfer versus chirp, with the period of the oscillations being related to structural properties of the ladder system. The situation, where the final state of the ladder is in the continuum, was examined by monitoring the direct three-photon ionization of the system.

ACKNOWLEDGMENTS

It is a pleasure to acknowledge the valuable assistance of B. Broers in the phase of constructing the experiment and setting up our initial calculations. R. C. Constantinescu is acknowledged for help with the laser system, T. Andersen and K. Mølmer for discussing various aspects of the theory, and H. B. van Linden van den Heuvell for critical reading of the manuscript. This work is part of the research program of the Stichting voor Fundamenteel Onderzoek der Materie (Foundation for Fundamental research on Matter), and was made possible by financial support of the Nederlandse Organisatie voor Wetenschappelijk Onderzoek (Netherlands Organization for the Advancement of Research).

APPENDIX: RELATIVE COUPLING STRENGTH TO CONTINUUM

The cross section for ionization by a linearly polarized laser beam from state $|\gamma\rangle$ of an atom to the $\varepsilon l'$ continuum leaving an ion in state $|\gamma'\rangle$ can be calculated as

$$\sigma(\gamma,\gamma'\varepsilon l')=K\frac{1}{g_\gamma}|\langle\gamma|\mathbf{e}_z\cdot\mathbf{D}|\gamma'\varepsilon l'\rangle|^2\ , \tag{A1}$$

where the constant K converts the square of the dipole moment to a cross section and depends on the applied normalization of the wave functions involved [with continuum wave functions normalized to energy, $K=4\pi^2/(3\hbar c)$] and g_γ is the degeneracy of the state $|\gamma\rangle$. Important in this context is the fact that under the assumption of LS coupling, the matrix element can be decomposed into an angular part and a reduced matrix element. Moreover, if we are dealing with one electron outside a closed shell, calculations are simplified further. For an atom interacting only with linearly polarized light, the value of the m quantum number is conserved. In our case, since the ground state is an s state, we thus have $m=0$ at all times. Starting out with the (multiplet

averaged) cross sections for ionization of the d state to the p and f continua, the square of the corresponding reduced matrix elements of the dipole operator (i.e., the line strengths) are easily calculated, since in this case the Wigner-Eckart theorem yields

$$\sigma(\gamma l,\varepsilon l')=K|\langle \gamma lm=0|\mathbf{e}_z\cdot\mathbf{D}|\varepsilon l'm=0\rangle|^2 =K\begin{pmatrix} l & 1 & l' \\ 0 & 0 & 0 \end{pmatrix}^2 |\langle \gamma l||D||\varepsilon l'\rangle|^2 , \tag{A2}$$

where we leave out $|\gamma'\rangle$, since the ion is simply left in its closed-shell ground state. In order to obtain the reduced matrix elements for each of the two fine-structure components, we make use of the coupling coefficients and the fact that the dipole matrix element is independent of spin. Then [16]

$$\langle \gamma slj\|D\|\varepsilon s'l'j'\rangle = \left[\frac{(2j+1)(2j'+1)}{(2s+1)}\right]^{1/2}\begin{Bmatrix} l & j & s \\ j' & l' & 1 \end{Bmatrix} \times\langle \gamma l\|D\|\varepsilon l'\rangle\delta_{s,s'} , \tag{A3}$$

where we have used the Racah $6j$ symbol. Using this formula, the reduced matrix element corresponding to each of the six couplings [Fig. 5(b)] can be calculated. The relative couplings to the continuum can now be obtained by again using the Wigner-Eckart theorem, but now for the fine-structure components (using $m_j=\pm\frac{1}{2}$):

TABLE II. Relative couplings of upper levels to continuum, $\mu_{n,j}$.

	$n=3$	$n=4$
$j=\frac{1}{2}$	$-\sqrt{5/12}\mu_p$	0
$j=\frac{3}{2}$	$-1/(2\sqrt{30})\mu_p$	$-3/(2\sqrt{5})\mu_p$
$j=\frac{5}{2}$	$\sqrt{7/15}\mu_f$	$1/(3\sqrt{70})\mu_f$
$j=\frac{7}{2}$	0	$\sqrt{10/21}\mu_f$

$$\langle \gamma sljm_j=\pm\tfrac{1}{2}|\mathbf{e}_z\cdot\mathbf{D}|\varepsilon s'l'j'm_j=\pm\tfrac{1}{2}\rangle = \begin{pmatrix} j & 1 & j' \\ \mp\frac{1}{2} & 0 & \pm\frac{1}{2} \end{pmatrix}\langle \gamma slj\|D\|\varepsilon s'l'j'\rangle . \tag{A4}$$

It is convenient to use the couplings related to the multiplet-averaged cross sections of ionization of $|\gamma\rangle=|5d,\ m=0\rangle$, so by fixing the phase of these couplings arbitrarily to zero, we let

$$\mu_p=\sqrt{|\langle 5d,l=2,m=0|\mathbf{e}_z\cdot\mathbf{D}|\varepsilon,l'=1,m=0\rangle|^2} , \qquad \mu_f=\sqrt{|\langle 5d,l=2,m=0|\mathbf{e}_z\cdot\mathbf{D}|\varepsilon,l'=3,m=0\rangle|^2} , \tag{A5}$$

satisfying

$$\sigma_p=K|\mu_p|^2 , \qquad \sigma_f=K|\mu_f|^2 , \tag{A6}$$

in which case the coupling $\mu_{n,j}$ as defined in Sec. V are as listed in Table II.

[1] W. S. Warren, H. Rabitz, and Mohammed Dahleh, Science **259**, 1581 (1993).
[2] R. N. Zare, Nature **365**, 105 (1993).
[3] For general references on femtosecond chemistry, see the feature issue *Femtosecond Chemistry: The Berlin Conference,* J. Phys Chem. **97**, 12 423 (1993).
[4] S. Chelkowski, A.D. Bandrauk, and P. B. Corkum, Phys. Rev. Lett. **65**, 2355 (1990).
[5] B. W. Shore, K. Bergmann, A. Kuhm, S. Schiemann, J. Oreg, and J. H. Eberly, Phys. Rev. A **45**, 5297 (1992).
[6] J. S. Mellinger, A. Hariharan, S. R. Gandhi, and W. S. Warren, J. Chem. Phys. **95**, 2210 (1991).
[7] J. S. Mellinger, S. R. Gandhi, A. Hariharan, J. X. Tull, and W. S. Warren, Phys. Rev. Lett. **68**, 2000 (1992).
[8] B. Broers, H. B. Van Linden van den Heuvell, and L. D. Noordam, Phys. Rev. Lett. **69**, 2062 (1992).
[9] L. D. Noordam, A. ten Wolde, A. Lagendijk, and H. B. van Linden van den Heuvell, Phys. Rev. A **40**, 6999 (1989).
[10] A. M. Weiner, J. P. Heritage, and E. M. Kirschner, J. Opt. Soc. Am. B **5**, 1563 (1988).
[11] A. A. Radzig and B. M. Smirnov, *Reference Data on Atoms, Molecules and Ions* (Springer-Verlag, Berlin, 1985).
[12] L. Allen and J. H. Eberly, *Optical Resonance and Two Level Atoms* (Dover, New York, 1975).
[13] E. B. Treacy, IEEE J. Quantum Electron **5**, 454 (1969).
[14] A. E. Siegman, *Lasers* (University Science, Mill Valley, CA, 1986).
[15] See, e.g., the overview by R. R. Freeman and P. H. Bucksbaum, J. Phys. B **24**, 325 (1991).
[16] I. I. Sobelman, *Atomic Spectra and Radiative Transitions* (Springer-Verlag, Berlin, 1992).
[17] H. G. Muller, Ph.D. thesis, Free University, Amsterdam, 1985.
[18] M. Aymar, E. Luc-Koenig, and F. Combet Farnoux, J. Phys. B **9**, 1279 (1976).

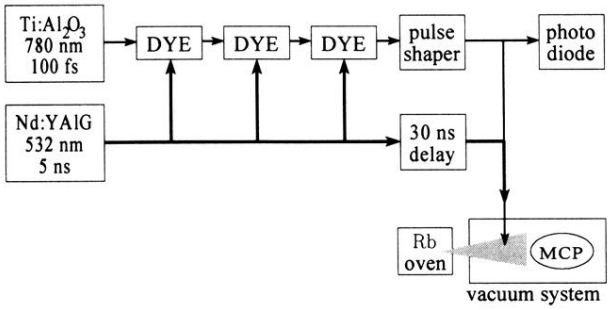

FIG. 2. A schematic of the experimental setup showing the laser system, pulse shaper, and the multi channel plate (MCP) detector in the vacuum chamber.